Combined effect of SDF-1 peptide and angiogenic cues in co-axial PLGA/gelatin fibers for cutaneous wound healing in diabetic rats

Muhammad Shafiq [a,b,*,1], Zhengchao Yuan [a,1], Muhammad Rafique [c], Shinichi Aishima [d], Hou Jing [e], Liang Yuqing [e], Hiroyuki Ijima [b], Shichao Jiang [e,f,**], Xiumei Mo [a,***]

[a] State Key Laboratory for Modification of Chemical Fibers and Polymer Materials, Shanghai Engineering Research Center of Nano-Biomaterials and Regenerative Medicine, College of Chemistry, Chemical Engineering and Biotechnology, Donghua University, Shanghai 201620, China
[b] Department of Chemical Engineering, Faculty of Engineering, Graduate School, Kyushu University, 744 Motooka, Nishi-ku, Fukuoka 819-0395, Japan
[c] State Key Laboratory of Medicinal Chemical Biology, College of Life Sciences, Nankai University, Tianjin, China
[d] Department of Pathology and Microbiology, Faculty of Medicine, Saga University, Nabeshima 5-1-1, Saga 849-8501, Japan
[e] Department of Orthopedics, Shandong Provincial Hospital Affiliated to Shandong First Medical University, Jinan 250021, China
[f] Medical Science and Technology Innovation Center, Shandong First Medical University & Shandong Academy of Medical Sciences, Jinan 250117, China

ARTICLE INFO

ABSTRACT

Skin regeneration is hindered by poor vascularization, prolonged inflammation, and excessive scar tissue formation, which necessitate newer strategies to simultaneously induce blood vessel regeneration, resolve inflammation, and induce host cell recruitment. Concurrent deployment of multiple biological cues to realize synergistic reparative effects may be an enticing avenue for wound healing. Herein, we simultaneously deployed SDF (stromal cell-derived factor)− 1α, VEGF (vascular endothelial growth factor)-binding peptide (BP), and GLP (glucagon like peptide)− 1 analog, liraglutide (LG) in core/shell poly(L-lactide-co-glycolide)/gelatin fibers to harness their synergistic effects for skin repair in healthy as well as diabetic wound models in rats. Microscopic techniques, such as SEM and TEM revealed fibrous and core/shell type morphology of membranes. Boyden chamber assay and scratch-wound assay displayed significant migration of HUVECs (human umbilical vein endothelial cells) in SDF-1α containing fibers. Subcutaneous implantation of membranes revealed higher cellular infiltration in SDF-1α loaded fibers, especially, those which were co-loaded with LG or BP. Implantation of membranes in an excisional wound model in healthy rats further showed significant and rapid wound closure in dual cues loaded groups as compared to control or single cue loaded groups. Similarly, the implantation of dressings in type 2 diabetes rat model revealed fast healing, skin appendages regeneration, and blood vessel regeneration in dual cues loaded fibers (SDF-1α/LG, SDF-1α/BP). Taken together, core/shell type fibers containing bioactive peptides significantly promoted wound repair in healthy as well as diabetic wound models in rats.

1. Introduction

Skin injuries caused by trauma or burn pose enormous psycho-social challenges. While skin exhibits intrinsic healing capacity, complications, including infection and diabetes may hinder *in situ* repair. Certain diseases, such as infection and diabetes may further worsen skin repair. Newer approaches aimed at improving vascularization *via* host cell mobilization may hold great promise for skin tissue engineering (TE). Angiogenic cues, such as vascular endothelial growth factor (VEGF) and basic fibroblast growth factor (bFGF) have been widely exploited for skin TE and shown to induce vascularization by promoting the migration, growth, and organization of endothelial cells (ECs) [1]. VEGF is an important angiogenic growth factor, which stimulates multiple phases of wound healing. However, it exhibits short half-life ($\sim$ 90 min) and
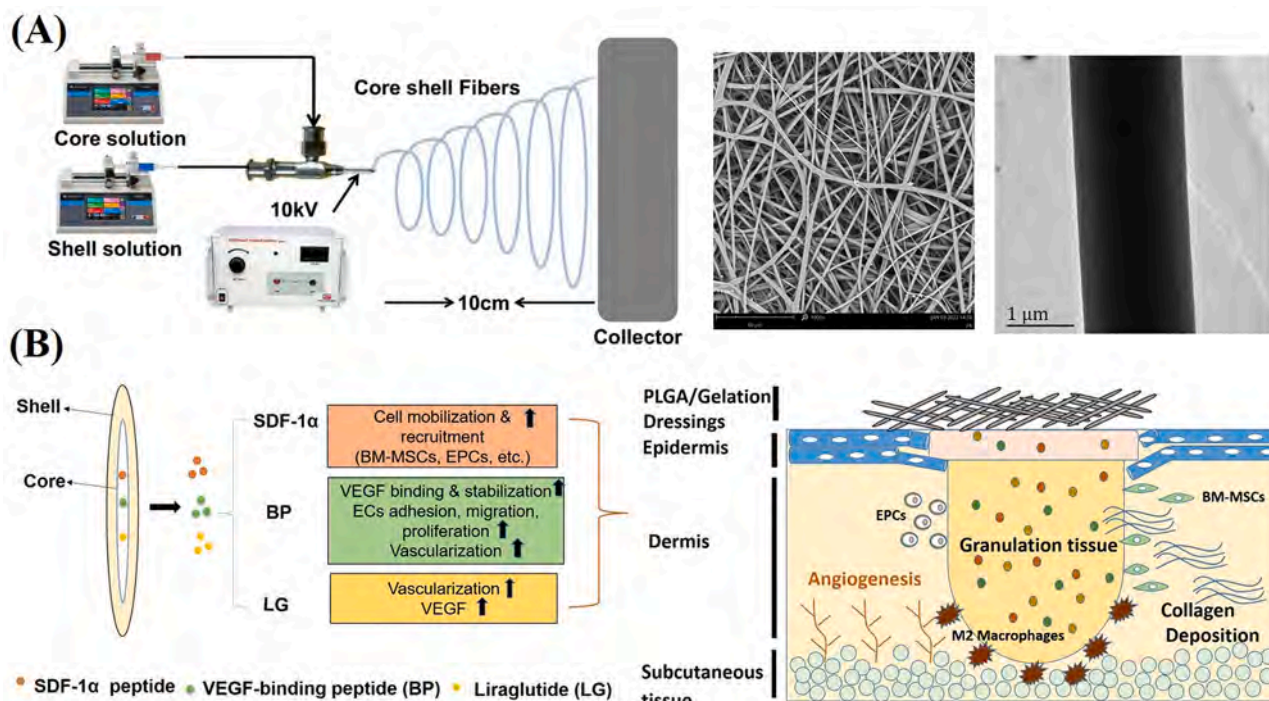

Scheme 1. Fabrication of core/shell fibers (A) and their application for cutaneous wound healing (B).

elevated levels of matrix metalloproteinases (MMPs) in chronic diabetic wounds further degrade growth factors (GFs), thereby necessitating frequent administrations [1]. Nonetheless, an overdose of VEGF may cause tumor-like vasculature formation, which necessitates additional bioactive cues to support VEGF-mediated tissue repair [2]. Short amino acid sequences, which may either replicate VEGF characteristics or recruit VEGF *in situ* also show angiogenic potential [3]. Radisch et al. reported significant re-epithelialization and wound closure in angiopoietin-1 derived peptide (QHREDGS) loaded dressings [4]. Similarly, Adini et al. discovered a 12-mer prominin-1-derived peptide (PR1P, herein named as BP), which significantly increased VEGF binding to ECs as well as increased angiogenesis by potentiating *endogenous* VEGF [5]. Moreover, BP promoted angiogenesis and tissue repair in different disease models, including excisional wounds, hind-limb ischemia, and damaged ligament tissues [6]. Nevertheless, bolus injection of BP or its simple encapsulation into fibers may hamper its utilization, which requires alternative approaches to enable its sustained release at injury site [6]. Glucagon like peptide-1 (GLP-1) analog, liraglutide (LG) has also been shown to promote the migration of several cell types, including keratinocytes and human umbilical vein endothelial cells (HUVECs) and promote skin repair through the expression of angiogenic GFs [7,8]. Nonetheless, poor water solubility and short half-life (~ 13 h) of LG limits its application in TE.

Unlike cell-based approaches, *in situ* TE through the mobilization and recruitment of endogenous stem/progenitor cells may have great application prospects [10,11]. Chemokines like stromal cell-derived factor 1-alpha (SDF-1α) promote *in situ* TE *via* improved vascularization and neo-tissue regeneration by recruiting multiple cell types, such as endothelial progenitor cells (EPCs) and smooth muscle progenitor cells (SMPCs) [9,12,13]. Tabata et al. observed significant skin repair, neovascularization, and epithelialization in excisional defects treated with SDF-1 overexpressing mesenchymal stem cells (MSCs) [10]. However, SDF-1α exhibits short half-life and is sensitive to MMPs and dipeptidyl peptidase-4 (DPP-4), which impede its application. SDF-1α-peptides were shown to overcome aforementioned limitations [14–16]. While endogenous cell recruitment may promote tissue repair through cellular differentiation or paracrine effect, additional cues may

be needed to further support SDF-1-mediated *in situ* TE. Guo et al. observed EPCs recruitment, differentiation, and endothelialization in SDF-1α/VEGF loaded conduits [17]. Mooney et al. co-loaded VEGF and SDF-1 into alginate hydrogels to promote EPC recruitment and subsequent neovascularization [18]. Consequently, angiogenic cues like VEGF-binding peptide (BP) and LG may support SDF-1α-mediated *in situ* tissue repair by promoting differentiation or paracrine secretion of recruited cells, thereby inducing neovascularization [7,8]. Since difficult-to-heal diabetic and infected wounds show delayed healing due to poor vascularization and prolonged inflammatory response, combined use of SDF-1α peptide and angiogenic cues (BP, LG) may hold great promise, which has not been explored yet. Consequently, the objective of this research was to discern the combined effect of SDF-1α and angiogenic molecules (BP, LG) to promote *in situ* repair of diabetic wounds (Scheme 1). We fabricated core/shell type poly(L-lactide-co--glycolide)/gelatin (PLGA/Gel) fibers containing either single cues like SDF-1α, LG, and BP or dual cues, such as SDF-1α/ LG and SDF-1α/BP. Incorporation of bioactive cues into core part of fiber may preserve their bioactivity and afford a sustained release (Scheme 1). After evaluation of the preliminary biocompatibility of dressings, they were applied to excisional wound defects in healthy and diabetic rat models. Membranes loaded with dual cues evidently showed rapid wound closure.

2. Experimental

2.1. Materials

Detail about materials has been summarized in Table S1 (Supporting Information). All other chemicals were of analytical grade and used as such without any further purification.

2.2. Fabrication of core/shell fibers

Core/shell fibers were fabricated by electrospinning (SS-3556 H, Yongkang Leye Technology Development Co., Ltd., Beijing, China) by using following parameters: co-axial needle, syringe pump size, 10 mL, voltage, 10 kV, flow rate, 0.1 mL/h and 1 mL/h for core and shell
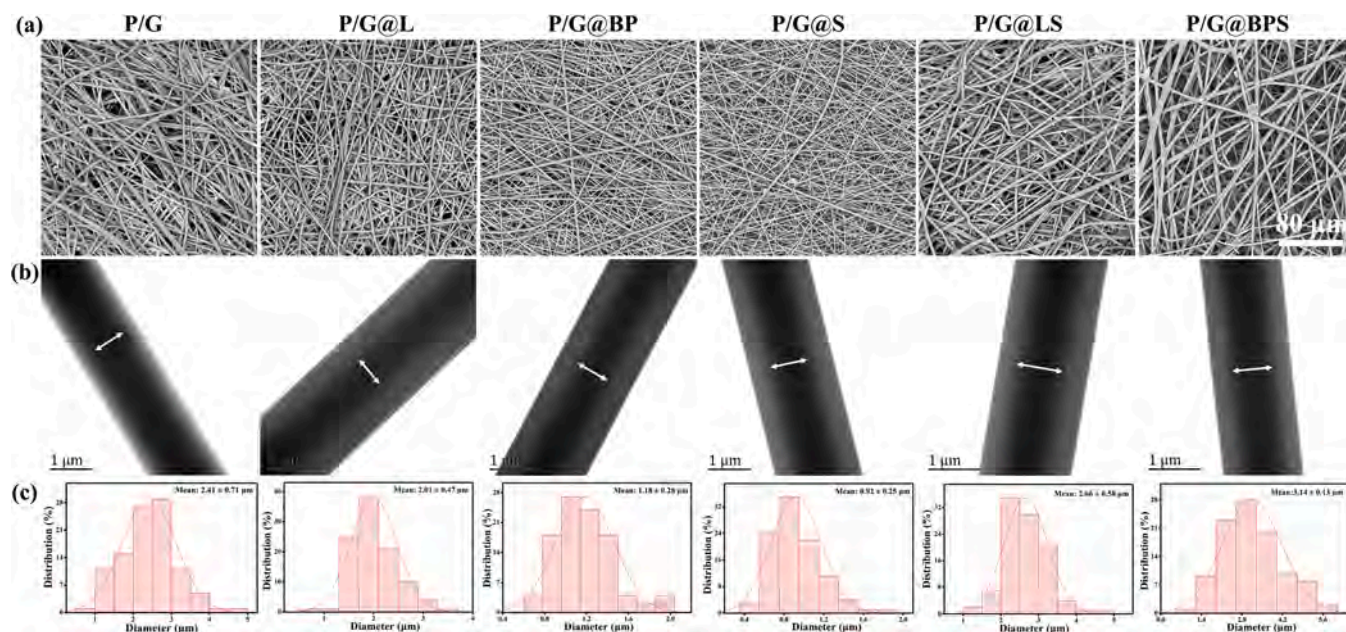
Fig. 1. Morphological analysis of membranes. SEM micrographs (a), TEM micrographs (b), and diameter distribution (c) of fibers. Scale bars, 80 μm (a) and 1 μm (b).

solutions, respectively, spinneret-to-collector distance, 10-cm, temperature, 25 °C, humidity, 45–50%, and aluminum foil collector. The PLGA/Gel (7:3, w/w) and organo essential oil (OEO, 10 wt% with respect to the total polymer weight) were dissolved in HFIP to afford 20% (w/v) shell solution, and stirred overnight at room temperature (RT). For core solutions, individual cues (LG, BP, SDF-1α, 1 mg, each) or dual cues (LG/SDF-1α or BP/SDF-1α, 1 mg, each) were dissolved in HFIP (1-mL) to fabricate P/G@L, P/G@BP, P/G@S, P/G@LS, and P/G@BPS membranes, respectively. For P/G (control group), HFIP and PLGA/Gel were used as core and shell solutions, respectively. Membranes were dried *in vacuo* for 3 days at RT.

2.3. Morphology of fibers

Membranes were sputter-coated with gold for morphological analysis by SEM (Hitachi, TM-1000, Japan). Average diameter of fibers ($n = 100$) was measured by Image J (v1.8.0, National Institutes of Health, USA). To discern core/shell morphology, TEM analysis was performed (JEM-2100, JEOL, Japan).

2.4. Biocompatibility of membranes

The biocompatibility was assessed by hemolysis assay, Boyden chamber assay, and scratch-wound assay *in vitro* [6]. The detailed procedures have been described in the supporting information.

2.5. Subcutaneous implantation of membranes

For preliminary biocompatibility, membranes were subcutaneously implanted in rats. 6-week-old SD rats were anesthetized by intraperitoneal (IP) injection of pentobarbital (45 mg.mL⁻¹). Ultraviolet (UV)-sterilized membranes were implanted into the dorsal pocket of rats ($n = 3$). At day 14, membranes along with their surrounding tissues were explanted, fixed in neutral buffered formalin, embedded in paraffin, and sectioned. Hematoxylin and Eosin (H&E) and Masson's Trichrome (MT) staining was performed following standard protocols.

2.6. Implantation of membranes in a healthy rat model

Animal experiments were performed following the guidelines of

Shandong Provincial Hospital Affiliated to Shandong First Medical University, Shandong, China. 6-week-old SD rats (weight = ~ 180 g, Jinan Pengyue Biotech Inc., Jinan, China) were anesthetized by IP injection of pentobarbital (45 mg.mL⁻¹). Dorsal area was totally depilated by Na₂S (8.0%, w/v) and four excisional defects (diameter, 10 mm) were created on the upper back of each rat. P/G, P/G@L, P/G@BP, P/G@S, P/G@LS, and P/G@BPS membranes were implanted ($n = 5$, each time point). Untreated wounds served as controls. Fresh membranes were used every three days. Wound size and wound closure (%) were measured by using ImageJ software (National Institutes of Health, v1.8.0, USA) at day 0, 4, 7, 10, and 14 post-operatively.

2.7. Implantation of membranes in a diabetic rat model

Diabetes was induced by a single IP injection of 60 mg.kg⁻¹ streptozotocin (STZ) dissolved in sodium citrate buffer (pH = 4.5). At day 3, whole-blood was collected from the tail vein, and glucose level was monitored by using a complete blood glucose monitor (Sinocare Biosensor Co., Changsha, China). Rats with glucose levels higher than 16.7 mM were transplanted with dressings similar to healthy model ($n = 5$, each time point). Wounds were imaged at day 0, 7, 14, and 21 post-operatively. Blood glucose level and body weight were measured every three days. The wound area was analyzed by tracing the wound margins and calculated by Image J. The wound closure rate (%) was expressed as a percentage of the original wound area and calculated by Eq. (1):

$$\text{Wound } area = \frac{E_t}{E_0} \times 100\% \tag{1}$$

The E_0 and E_t represent the wound size at day 0 and at designated time intervals, respectively. Scar length was calculated as the ratio between the distance covered by the epithelium and the distance between wound ends by using Image J.

2.8. Histological analysis and immunofluorescence staining

At each time point, animals were euthanized by carbon dioxide (CO₂) asphyxiation; surrounding skin and muscle, including the wound areas were removed and processed for H&E and MT staining (applied to both the healthy and diabetic models). Explants from diabetic rats were
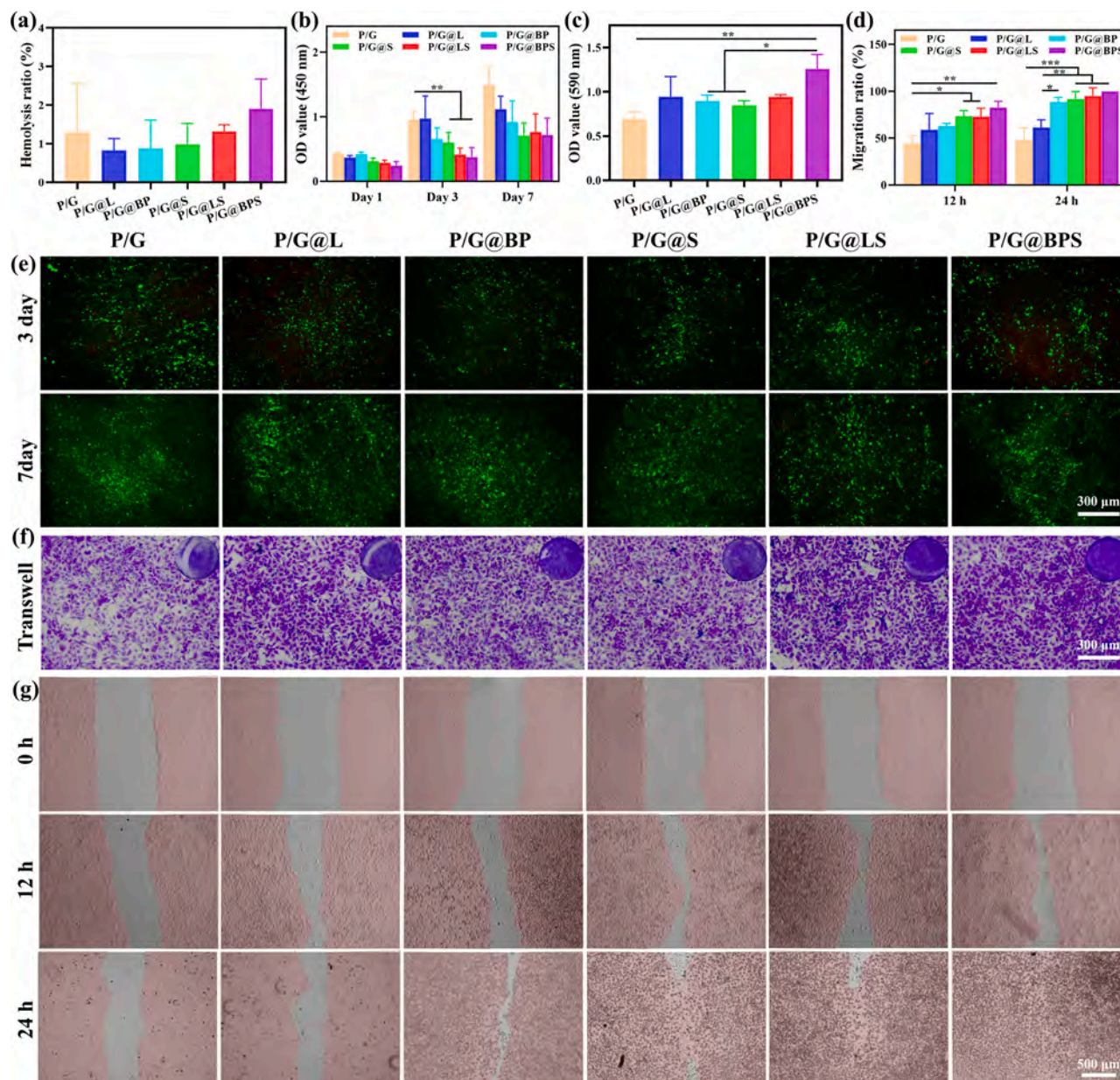
Fig. 2. Cytocompatibility of membranes *in vitro*. Hemolysis ratio (a), proliferation of HUVECs (b), migration ratio of cells in a scratch-wound assay *in vitro* (c), OD value (590 nm) of the migrated cells in Boyden chamber assay (d), live/dead cell assay (e), Transwell migration assay (f), and scratch-wound assay *in vitro* (f). Scale bars, 300 μm (e—f) and 500 μm (g).

also stained with immunofluorescence (IF) staining for CD31, alpha-smooth muscle actin (α-SMA), CD68, CD206, and picrosirius red (PSR). ImageJ software was used to quantify the numbers of positive cells or positive areas in each field of view. Main organs from diabetes model, including heart, liver, spleen, lung, and kidney were also analyzed by H&E staining.

2.9. Statistical analysis

Data were expressed as mean ± standard deviation. All data were analyzed by one-way ANOVA with Tukey's *post hoc* tests. Statistical significance was considered at $p < 0.05$ and $p < 0.01$.

3. Results

3.1. Morphological analysis

Fig. 1 shows SEM and TEM micrographs of membranes. Bead-free fibers bearing a smooth surface were formed (Fig. 1A). TEM displayed core/shell morphology of fibers (Fig. 1B). The average diameter of fibers was 2.41 ± 0.71 μm, 2.01 ± 0.47 μm, 1.18 ± 0.28 μm, 0.92 ± 0.25 μm, 2.66 ± 0.58 μm, and 3.14 ± 0.13 μm in P/G, P/G@L, P/G@BP, P/G@S, P/G@LS, and P/G@BPS membranes, respectively (Fig. 1C).

3.2. Biocompatibility of membranes

Preliminary biocompatibility of membranes was evaluated by different assays *in vitro*. All groups showed negligible hemolysis ratio (< 2%), which well-conforms international standard of < 5% of hemolysis [18].
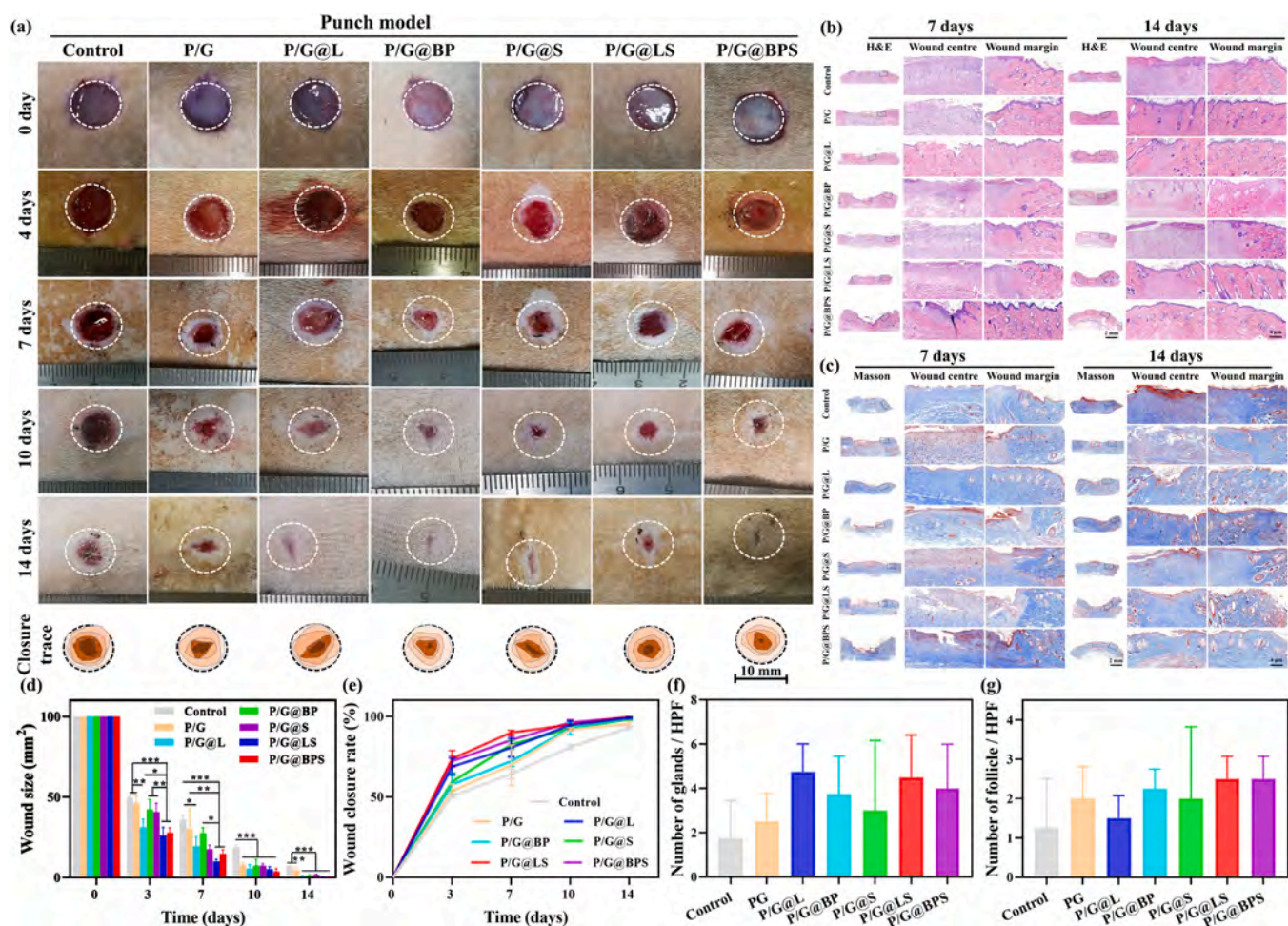
Fig. 3. Membranes promoted wound healing in excisional defects in healthy rats. Representative photographs showing wound closure for up to 14 days (a). H&E (b) and Masson's trichrome staining (c) of wounds center and margins at day 7 and 14. Wound size at each time point normalized with respect to the wound size at day 0 (d). Wound healing rate concomitantly increased for up to day 14 (e). There was an insignificant difference among different groups in terms of the number of glands and hair follicles per hpf (f—g) at day 14 post-operatively. Scale bars, 2 mm and 4 μm (b—c).

The CCK-8 assay showed an increase in cell proliferation over 7 days. There was insignificant difference among various groups in terms of cell proliferation at day 1 and 7. The PG@LS and PG@BPS showed slightly less cell proliferation than other groups at day 3 (Fig. 2b). Live/dead staining also showed good cell viability on all scaffolds without an obvious apoptosis for up to day 7 (Fig. 2e).

In Boyden chamber assay, P/G recruited only a few numbers of HUVECs. In contrast, membranes containing SDF-1α, BP, and LG recruited significantly more number of cells (Fig. 2c, f). Similarly, in a scratch-wound assay, P/G@S, P/G@LS, and P/G@BPS exhibited remarkably higher migration of HUVECs at both 12 and 24 h (Figs. 2g & S2).

3.3. Subcutaneous implantation of membranes

H&E and MT staining of the native skin showed intact epidermis, hair follicles, well-organized collagen tissues, and blood vessels (Fig. S3). By day 14, while all subcutaneously implanted groups were populated with host cells, those containing SDF-1α (P/G@S, P/G@LS, P/G@BPS) exhibited more number of infiltrated cells (Fig. S4). Besides, MT staining revealed excessive infiltration of host cells as well as significant regeneration of collagen and blood vessels in SDF-1α containing membranes (P/G@S, P/G@LS, P/G@BPS).

3.4. Implantation of membranes in excisional defects in healthy rats

Fig. 3 showed photographs of healed wounds and histological analysis over day 14. Wounds treated with bioactive dressings had substantially healed as observed by wound photographs and closure trace analysis (Fig. 3a). In contrast, wound healing was still ongoing in control and P/G groups, which exhibited partially healed wounds (Fig. 3a, d). At all-time points, wounds treated with bioactive dressings, especially, those with combination groups (P/G@LS, P/G@BPS) showed significantly less wound size and substantial wound closure percentages than that of the control and P/G groups (Fig. 3d—e).

H&E staining further revealed that wounds in control and P/G groups were not fully repaired by day 7 (Fig. 3b). As compared to other groups, wounds in P/G@BPS group showed a clean wound bed with mild inflammation in wound center and margin (Fig. 3b). By day 14, while all wounds exhibited re-epithelialization and granulation tissue regeneration, the control and P/G groups still showed inflammation in wound center (Fig. 3b). Furthermore, MT staining showed an intact skin in bioactive dressing groups at day 14 than other groups (Fig. 3c). Number of hair follicles and glands also showed an increasing trend with implantation time.

H&E and MT staining micrographs were also evaluated for pathological parameters and representative pictures have been marked (Fig. S5 & Table S2). P/G@BP groups showed complete epithelialization, dermal regeneration, appendages formation, and collagen
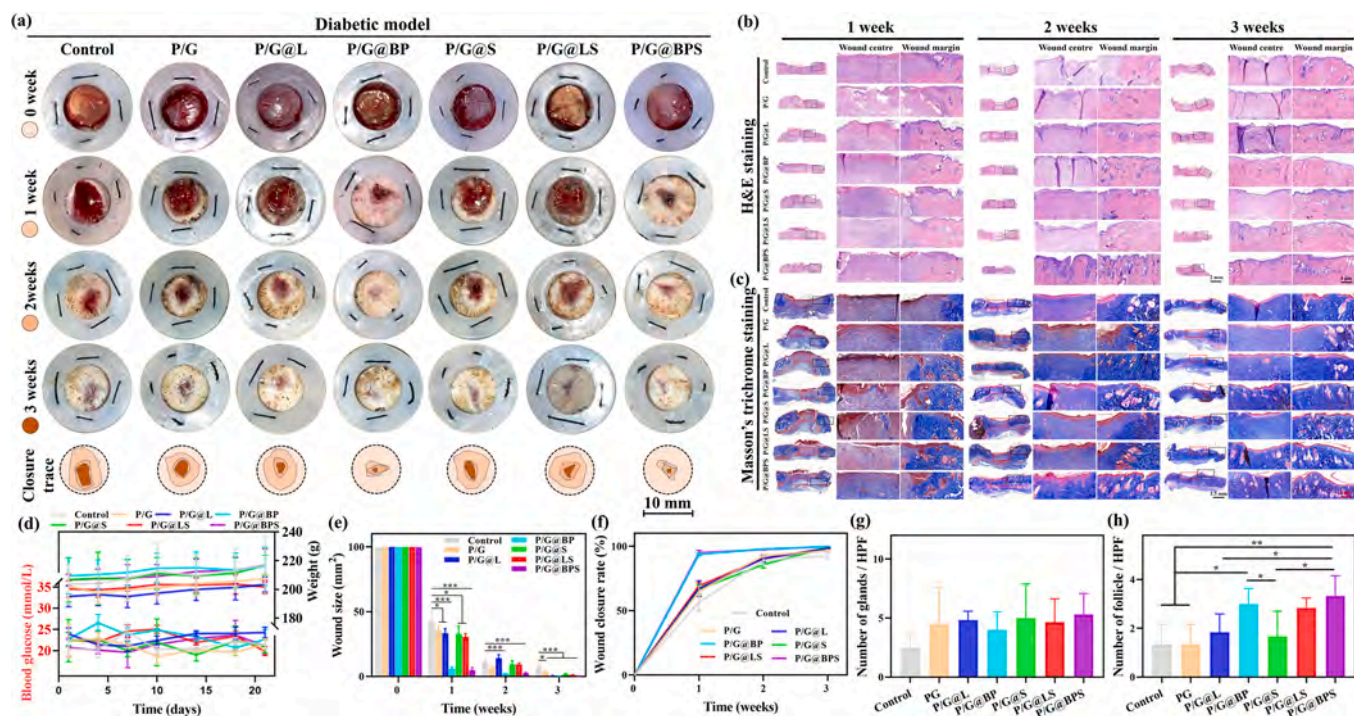
Fig. 4. Implantation of membranes in a full-thickness excisional skin defect model in diabetic rats for up to 3 weeks. Untreated wounds served as controls. Representative photographs showing wound size (a). H&E staining (b) and Masson's trichrome staining (c) of wound center and margin. (d) Blood glucose and body weight of rats receiving different membranes. Wound size at each time point normalized with respect to day 0. Wound closure rate (%) (f). Number of glands (g) and hair follicles (h) per hpf by day 21. Scale bars, 2 mm and 4 μm (b—c).

regeneration, while lacked granulation tissue formation and inflammation 14 days post-operatively. The P/G@BPS group exhibited healed or preserved epithelialization as well as healed dermal regeneration and appendages formation, while granulation tissues and inflammation were either absent or were only mild. Similarly, P/G@LS group displayed moderate or preserved epithelialization, mild or focal granulation tissues, moderate dermal regeneration, and moderate or healed appendages regeneration along with mild or focal inflammation. The P/G@BPS and P/G@LS groups also showed preserved collagen regeneration both at day 7 and 14.

3.5. Implantation of membranes in excisional defects in a diabetic rat model

We next ascertained the potential of dressings in a Type 2 diabetic rat model. Fig. 4 shows photographs of diabetic wounds and their histological analysis over 3 weeks. Body weight of rats gradually increased in all groups, while blood glucose level showed some fluctuations (Fig. 4d). Wounds in all groups displayed gradual healing over time; P/G@BP and P/G@BPS treated defects showed fast healing (Fig. 4e). Similarly, wounds treated with bioactive dressings groups showed significantly higher wound closure rate as compared to control and P/G group.

By week 1, H&E staining of wound tissues in control and P/G groups manifested unhealed wound portions and incomplete epithelialization, especially, in the wound center (Fig. 4b). By week 2, sections from control and P/G groups still revealed unhealed wound portions as well as incomplete epithelialization. In contrast, wounds treated with bioactive dressings had significantly healed and exhibited epithelialization. Intriguingly, wounds treated with the P/G@BP, P/G@LS, and P/G@BPS membranes showed more number of blood vessels than other groups; P/G@BPS also exhibited significant hair follicle regeneration. By week 3, wounds in control, P/G and P/G@L groups were either healed incompletely or showed scar tissues, especially, in the wound center. Contrarily, P/G@S, P/G@LS, and P/G@BPS groups exhibited

scarless tissue repair along with the clear wound bed, more number of blood vessels, and hair follicles. MT staining further showed regular and orderly collagen deposition as well as significant appendages formation (glands, hair follicles) in P/G@L, P/G@BP, P/G@S, P/G@LS, and P/G@BPS treated wounds than that of the control and P/G groups 3 weeks post-operatively.

H&E and MT staining micrographs were next examined for the extent of regeneration. Control group exhibited mild or focal epithelialization, dermal regeneration, appendages regeneration, while severe granulation and inflammation 7 days post-operatively. P/G@BP, P/G@S, P/G@BPS, and P/G@LS exhibited healed or preserved epithelialization, dermal regeneration, and collagen regeneration at all-time points (Table S3). The P/G@S and P/G@LS displayed no or mild inflammation at all-time points. The representative pictures have also been marked for pathological parameters (Fig. S6, Supporting Information).

3.6. Blood vessel regeneration

Fig. 5 shows co-staining of explants with CD31/α-SMA to ascertain blood vessel regeneration. Control and P/G groups showed many CD31+ cells, however, there were only a few number of CD31+/α-SMA+ blood vessels in the wound center at 1-wk. P/G@L and P/G@S displayed slightly higher number of CD31+/α-SMA+ blood vessels than control and P/G groups (Fig. 5a). The P/G@BP group showed more number of CD31+/α-SMA+ blood vessels as compared to control, P/G, and P/G@L groups. Noticeably, P/G@LS and P/G@BPS exhibited significantly higher number of CD31+/α-SMA+ blood vessels in the wound center. Quantitative analysis also revealed significantly higher numbers of blood vessels in P/G@BP, P/G@LS, and P/G@BPS than other groups by 1-wk (Fig. 5b). P/G@BP, P/G@LS, and P/G@BPS groups showed the highest number of the matured blood vessels (CD31+/α-SMA+) than that of the other groups (Fig. 5c).
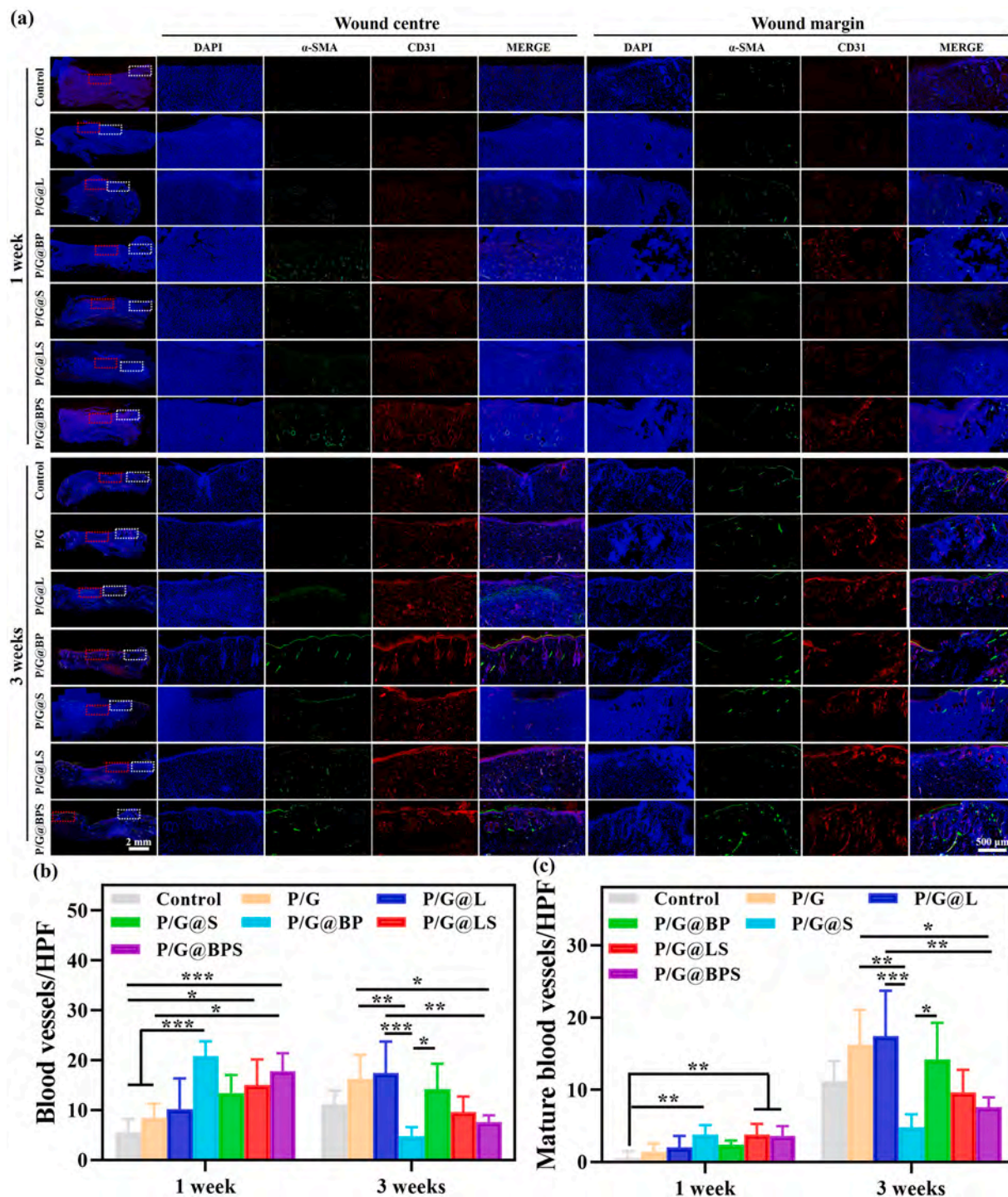
Fig. 5. Angiogenesis at wound centers and margins of diabetic rat model at day 7 and 21 receiving different membranes. IF staining of α-SMA (green) and CD31 (red) at day 7 and 21 (a), Scale bars, 2 mm and 500 μm. Number of blood vessels (b), and mature blood vessels (c) in the wounds at day 7 and 21.

3.7. Immunomodulation

To explore immunomodulatory effect, explants were stained for CD68^{+} and CD206^{+} macrophages (Fig. 6). There was insignificant difference among groups for CD68^{+} macrophages by week 1. Contrarily, P/G@BP, P/G@S, P/G@LS, and P/G@BPS treated wounds displayed more number of CD206^{+} macrophages than that of the control and P/G groups at week 1. By week 3, P/G@BP exhibited significantly less number of CD68^{+} macrophages than other groups (Fig. 6a—c). However, there was an insignificant difference among groups for CD206^{+} macrophages at 3-

wk. The P/G@BP groups also exhibited higher ratio of CD206^{+}/CD68^{+} macrophages as compared to other groups at 3 weeks post-operatively (Fig. 6d). These data indicated that bioactive dressings may have an immunomodulatory effect, which may have implications for earlier wound repair.

3.8. Deposition of collagen

Collagen deposition was ascertained by PSR staining. By week 1, all groups exhibited negligible collagen deposition in the wound center
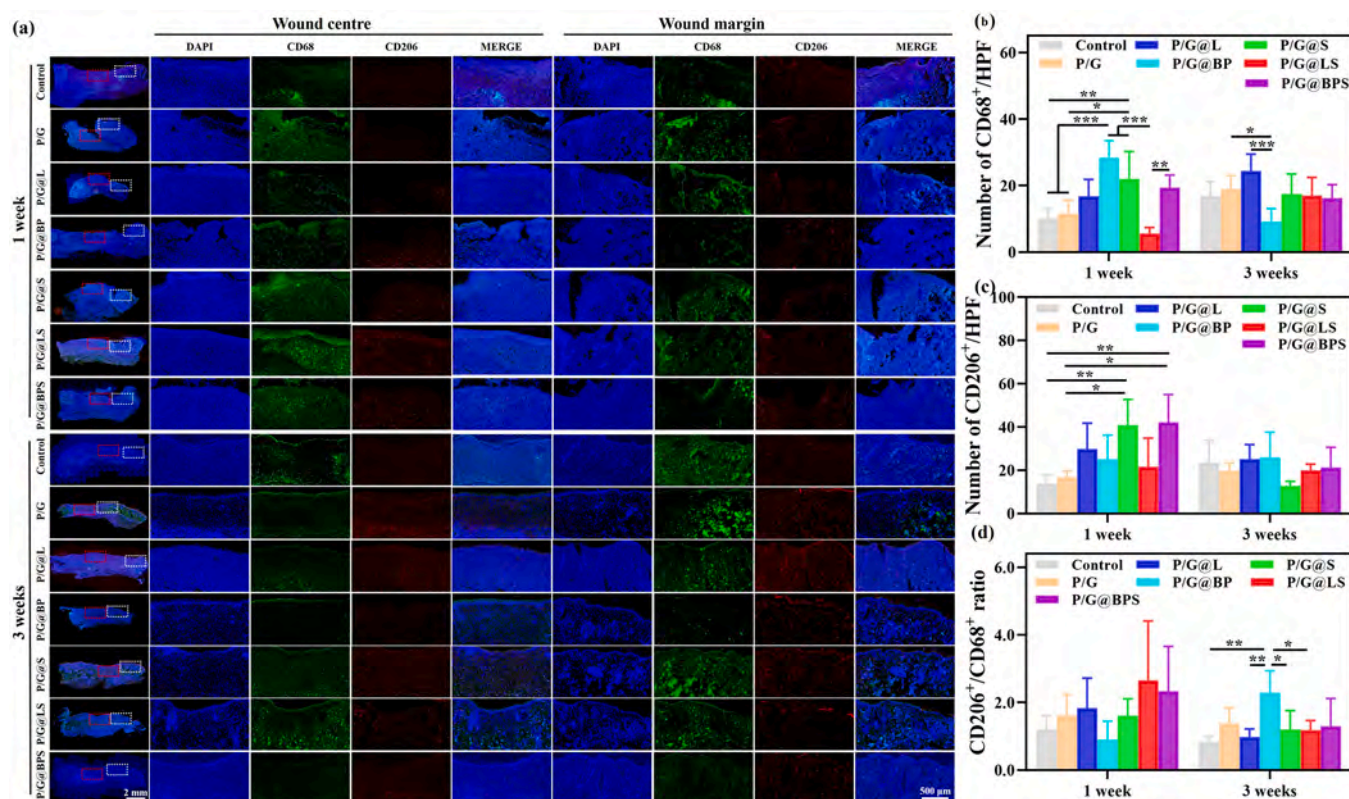
Fig. 6. Inflammatory response at wound center and margin of diabetic rat model receiving different membranes at day 7 and 21. IF staining for CD68 (green) and CD206 (red) at day 7 and 21 (a). Number of CD68$^+$ macrophages (b), CD206$^+$ macrophages (c), and CD206$^+$/CD68$^+$ macrophages (d). Scale bars, 2 mm and 500 μm.

(Fig. 7). While control, P/G, P/G@L, and P/G@BP groups exhibited disorganized collagen regeneration mainly at the wound edges, P/G@LS and P/G@BPS groups displayed accumulation of collagen even at wound edges. Strikingly, by 3 weeks, groups that received bioactive membranes (*e.g.*, P/G@L, P/G@BP, P/G@S, P/G@LS, and P/G@BPS) showed nice regeneration of collagen at the wound center than control and P/G groups, which only showed marginal collagen deposition (Fig. 7a). Bioactive dressings enabled collagen regeneration even in the wound center by 3 weeks, thereby indicating their potential to improve re-epithelialization over untreated and P/G groups.

Moreover, histological analysis of main organs like heart, liver, spleen, lung, and kidney from all groups did not reveal significant alterations by week 3, demonstrating the safety of dressings (Fig. 7b).

4. Discussion

Neovascularization may improve viability and functionality for skin TE. As skin regeneration is a dynamic process, multiple GFs have been harnessed to facilitate regeneration of damaged skin tissues. VEGF delivery in skin models improved neovascularization and granular tissue formation [1,19]. Similarly, SDF-1α enhanced wound healing by recruiting different types of cells, including BM-MSCs, CD34$^+$ EPCs, and HSCs and promoting neovascularization in healthy and diabetic rat models [20]. Penn et al. observed significant wound closure in SDF-1 protein treated wounds in Yorkshire pigs than sham or control [20]. However, protein-based therapies are limited due to extensive degradation and short half-life when a bolus form of GFs is delivered *in vivo*. Short amino-acid sequences capable of replicating function of their full-length proteins may obviate abovementioned limitations [5,14–17]. We and others reported notable effects of angiogenic BP and LG as well as SDF-1α; BP induced anti-inflammatory response, neovascularization, and re-epithelialization in healthy and diabetic wound models, LG promoted skin repair in bacterial-infected wounds, and SDF-1α

facilitated neo-vessel formation and host cell recruitment [6,8,16]. Nevertheless, mere encapsulation of bioactive cues into fibers may confine their bioactivity. While, abovementioned cues exhibit distinct functions, their synergistic effects were not explored. Herein, we leveraged co-axial electrospinning to afford core/shell type fibers. Since diabetic skin repair is relatively slower than normal wounds, incorporation of BP, LG, and SDF-1α into core may ensure long-term release; dual cues can also be incorporated separately into core and shell parts to realize spatio-temporal release, which has previously been shown to promote tissue repair [21]. Microscopic analysis revealed core/shell type morphology of fibers.

Since dressings directly interact with wound tissues, biocompatibility evaluation is of considerable significance. Bioactive cues may lose their bioactivity due to harsh processing conditions during electrospinning. In vitro biological assays showed negligible hemolysis ratio and cytocompatibility as well as tube formation and migration of HUVECs, which corroborated our prior reports [8,16,21,22]. Previously, we incorporated varying concentrations of LG (0.05, 0.10, 0.15%, w/w) in PLGA/Gel fibers, which showed good cell growth over time [8]. Yu et al. prepared PLGA/Gel fibers with 5% (w/v) LG, which improved proliferation, tube formation, and migration of HUVECs and were ascribed to LG-mediated VEGF production [23]. Similarly, we prepared PLGA/Gel fibers containing different content of BP (0.002, 0.02, 0.2 mg), which displayed concentration-dependent effect to promote tube formation in ECs and wound healing *in vitro* [22]. Besides, we immobilized BP on the surface of PCL/Gel fibers, which also promoted growth, tube formation, and migration of HUVECs [6]. BP is a 12-mer peptide sequence, which potentiates VEGF *in situ* and augments its signaling within local wound microenvironments [5,24]. SDF-1α is a potent chemoattractant of multiple cells and has been shown to promote vascularization and tissue repair in different injury models [1,9,14–17, 20]. P/G@S, P/G@LS, and P/G@BPS groups showed significant migration of HUVECs in both scratch-wound assay and Boyden chamber
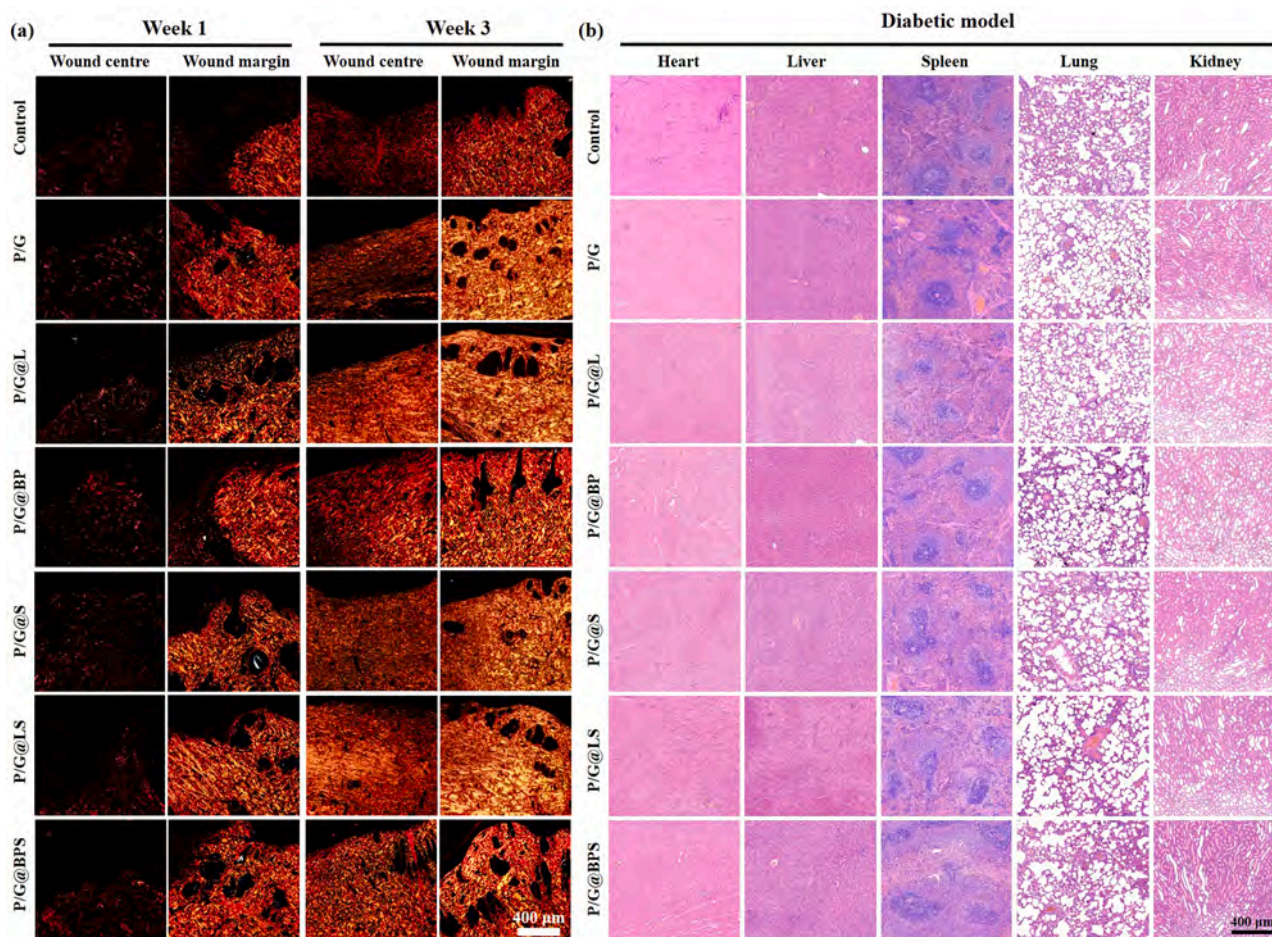
Fig. 7. Collagen maturation and visceral toxicity of diabetic rat model receiving different membranes. (a) Picrosirius Red (PSR) staining at day 7 and 21, Scale bars, 400 μm. (b) H&E-stained sections of main organs collected from diabetic rat model after different treatments for 21 days. Scale bars, 400 μm.

assay, which is also in agreement with above reports.

Since wound healing is a dynamic process, multiple GFs and cells participate in repair process [1,25]. Injury leads to overexpression of chemoattractants, which drive endogenous cell recruitment [11,12,22]. However, due to MMPs, GFs undergo degradation [10,14,15]. We and others previously reported that exogenous BP mediates its therapeutic effects *via* VEGF and its receptors (VEGFR) and enhances VEGF recruitment and stabilization *in vivo*, thereby inducing neovascularization [6,22]. Besides, LG and SDF-1α were shown to promote tissue repair by inducing neo-vessel regeneration and stem cell recruitment, respectively [8,16]. Implantation of membranes in subcutaneous and excisional defect models in healthy rats showed profound recruitment of host cells and rapid wound closure in SDF-1α containing groups, especially those loaded with dual cues (P/G@LS, P/G@BPS), which may be ascribed to synergistic effect of SDF-1α with LG and BP. Previously, GFs, such as VEGF and bone morphogenetic protein-2 (BMP-2) have been used with substance P and SDF-1α to harness synergistic effect [2, 17,18,26,27]. Consequently, endogenous recruitment of host cells and neovascularization may have played a pivotal role for wound healing. We think that the SDF-1α can recruit host cells, while BP and LG can improve angiogenesis, both of these processes may act concertedly to improve skin repair [5,8,17].

Since wound healing is impaired in diabetes, which is further exacerbated by poor vascularization, bioactive cues capable of promoting neovascularization may hold great promise [28,29]. All studied bioactive cues (BP, LG, SDF-1α) have been shown to promote skin repair in diabetic models [22,23,30]. BP induced wound healing in healthy and diabetic rat models by recruiting VEGF and promoting

anti-inflammatory phenotype of macrophages [22]. Besides, BP has been shown to promote vascularization and tissue repair in multiple injury models, including choroidal neovascularization, hind-limb ischemia, and degenerated ligament tissues, which were ascribed to its potentials to promote VEGF stabilization as well as increased proliferation, migration, and organization of ECs [5,6,31]. Similarly, LG promoted diabetic skin repair by increasing VEGF production of HUVECs while downregulating the level of miR-29b-3p; the latter was mediated by AKT/GSK-3β/β-catenin pathway [23]. SDF-1α is a potent cytokine, which can mobilize and recruit host cells, and promote tissue repair by inducing the differentiation of recruited cells into targeted lineages or promoting paracrine effects [17,32]. We also observed rapid wound closure and evidently higher vascularization in diabetic wound model in P/G@BP, P/G@LS, and P/G@BPS groups; the latter also exhibited significant hair follicle regeneration. Similarly, bioactive dressing groups showed scarless wound healing manifesting significant appendages regeneration than control and PG group. Moreover, P/G@BP, P/G@LS, and P/G@BPS displayed more number of CD206^{+} cells than other groups, which is indicative of their immunomodulatory potential [33, 34]. The higher wound closure in dual cues loaded groups may in part be ascribed to obviously higher neovascularization and immune-modulation in these groups, which is also in agreement with previous literature [22,23,30,31]. As mentioned before, while SDF-1α, BP, and LG were previously shown to promote diabetic wound healing, their combined effect was not studied.

This research has also some limitations. First, while we deciphered morphology of membranes by SEM and TEM as well as indirectly assessed the stability and bioactivity of incorporated cues,

characterization of the membrane for kinetics release, loading efficiency, chemical composition, wettability, degradation profile, mechanical stability, permeability yet remain to be done. Second, while different cell types participate in skin repair (fibroblasts, keratinocytes, ECs), we only exploited HUVECs for biological assays [35]. Evaluation with other cell types yet remains to be done. Third, as ROS and bacterial species obscure wound healing, determination of anti-oxidative and antibacterial properties is warranted [36]. Fourth, mechanistic insight about the synergistic effect between LG/SDF-1α or BP/SDF-1α needs to be further deciphered [37].

5. Conclusions

Altogether, we fabricated core/shell fibers to reveal synergistic effect of LG or BP along with SDF-1α; the latter was used owing to its ability to mobilize/recruit endogenous cells, while LG and BP were exploited to further support tissue repair due to their evident angiogenic effects. Membranes containing SDF-1α peptide (P/G@S, P/G@LS, P/G@BPS) showed higher cell migration and wound healing *in vitro* as well as induced more cell infiltration in a subcutaneous model in rats than other groups. Dual peptides loaded membranes (P/G@BPS) also displayed significant wound closure than untreated wounds or those treated with P/G or single bioactive cues. P/G@BP and P/G@BPS membranes also induced fast healing in a diabetic wound model in rats; P/G@LS and P/G@BPS were superior to the other groups in skin appendages (hair follicles and glands) and CD31$^+$/α-SMA$^+$ blood vessels. Core/shell fibers containing bioactive peptides significantly promoted wound repair in healthy as well as diabetes wound models, which may have implications for wound repair as well as other related disciplines.

CRediT authorship contribution statement

Muhammad Shafiq: Conceptualization, Methodology, Formal analysis, Resources, Data curation, Writing – original draft, Writing – review & editing, Project administration, Funding acquisition. **Zhengchao Yuan:** Methodology, Software, Formal analysis, Data curation. **Muhammad Rafique:** Conceptualization, Methodology, Writing – original draft. **Shinichi Aishima:** Methodology, Investigation. **Hou Jing:** Software, Methodology. **Liang Yuqing:** Software, Formal analysis, Methodology. **Hiroyuki Ijima:** Validation, Investigation, Resources, Visualization. **Shichao Jiang:** Validation, Resources, Data curation, Visualization, Project administration, Funding acquisition. **Xiumei Mo:** Validation, Resources, Visualization, Supervision, Project administration, Funding acquisition.

Declaration of Competing Interest

The authors declare that they have no known competing financial interests or personal relationships that could have appeared to influence the work reported in this paper.

Data availability

Data will be made available on request.

Acknowledgments

Appendix A. Supplementary material

Supplementary data associated with this article can be found in the online version at doi:10.1016/j.colsurfb.2023.113140.

References

[1] A. Joshi, Z. Xu, Y. Ikegami, K. Yoshida, Y. Sakai, A. Joshi, T. Kaur, Y. Nakao, Y. I. Yamashita, H. Baba, S. Aishima, Exploiting synergistic effect of externally loaded bFGF and endogenous growth factors for accelerated wound healing using heparin functionalized PCL/gelatin co-spun nanofibrous patches, J. Chem. Eng. 15 (404) (2021), 126518.

[2] L. Antonova, A. Kutikhin, V. Sevostianova, E. Velikanova, V. Matveeva, T. Glushkova, A. Mironov, E. Krivkina, A. Shabaev, E. Senokosova, L. Barbarash, bFGF and SDF-1α improve in vivo performance of VEGF-incorporating small-diameter vascular grafts, Pharmaceuticals 14 (4) (2021) 302.

[3] N.A. Impellitteri, M.W. Toepke, S.K. Levengood, W.L. Murphy, Specific VEGF sequestering and release using peptide-functionalized hydrogel microspheres, Biomaterials 33 (12) (2012) 3475–3484.

[4] Y. Xiao, L.A. Reis, N. Feric, E.J. Knee, J. Gu, S. Cao, C. Laschinger, C. Londono, J. Antolovich, A.P. McGuigan, M. Radisic, Diabetic wound regeneration using peptide-modified hydrogels to target re-epithelialization, Proc. Nat. Acad. Sci. USA 113 (40) (2016) E5792–E5801.

[5] A. Adini, H. Wu, D.T. Dao, V.H. Ko, L.J. Yu, A. Pan, M. Puder, S.Z. Mitiku, R. Potla, H. Chen, J.M. Rice, PR1P stabilizes VEGF and upregulates its signaling to reduce elastase-induced murine emphysema, Am. J. Respir. Cell. Mol. Biol. 63 (4) (2020) 452–463.

[6] Z. Yuan, D. Sheng, L. Jiang, M. Shafiq, R. Hashim, Y. Chen, B. Li, X. Xie, J. Chen, Y. Morsi, X. Mo, Vascular endothelial growth factor-capturing aligned electrospun polycaprolactone/gelatin nanofibers promote patellar ligament regeneration, Acta Biomater. 140 (2022) 233–246.

[7] J. Wu, G.R. Williams, C. Branford-White, H. Li, Y. Li, L.-M. Zhu, Liraglutide-loaded poly(lactic-co-glycolic acid) microspheres: preparation and in vivo evaluation, Eur. J. Pharm. Sci. 92 (2016) 28–38.

[8] F. Wu, Z. Yuan, M. Shafiq, L. Zhang, M. Rafique, F. Yu, E.N. Mohamed, E.H. Hany, Y. Morsi, Y. Xu, X. Mo, Synergistic effect of glucagon-like peptide-1 analogue liraglutide and ZnO on the antibacterial, hemostatic, and wound healing properties of nanofibrous dressings, J. Biosci. Bioeng. 134 (3) (2022) 248–258.

[9] J. Yu, A. Wang, Z. Tang, J. Henry, B.L. Lee, Y. Zhu, F. Yuan, F. Huang, S. Li, The effect of stromal cell-derived factor-1α/heparin coating of biodegradable vascular grafts on the recruitment of both endothelial and smooth muscle progenitor cells for accelerated regeneration, Biomaterials 33 (32) (2012) 8062–8074.

[10] Y. Nakamura, H. Ishikawa, K. Kawai, Y. Tabata, S. Suzuki, Enhanced wound healing by topical administration of mesenchymal stem cells transfected with stromal cell-derived factor-1, Biomaterials 34 (2013) 9393–9400.

[11] M. Shafiq, S.H. Kim, Biomaterials for host cell recruitment and stem cell fate modulation for tissue regeneration: focus on neuropeptide substance P, Macromol. Res. 24 (11) (2016) 951–960.

[12] M. Shafiq, O. Ali, S.B. Han, D.H. Kim, Mechanobiological strategies to enhance stem cell functionality for regenerative medicine and tissue engineering, Front. Cell Dev. Biol. 9 (2021), 747398.

[13] M. Shafiq, S.H. Kim, Covalent immobilization of MSC-affinity peptide on poly (L-lactide-co-ε-caprolactone) copolymer to enhance stem cell adhesion and retention for tissue engineering applications, Macromol. Res. 24 (11) (2016) 986–994.

[14] V.F. Segers, T. Tokunou, L.J. Higgins, C. MacGillivray, J. Gannon, R.T. Lee, Local delivery of protease-resistant stromal cell derived factor-1 for stem cell recruitment after myocardial infarction, Circulation 116 (15) (2007) 1683–1692.

[15] M. Shafiq, D. Kong, S.H. Kim, SDF-1α peptide tethered polyester facilitates tissue repair by endogenous cell mobilization and recruitment, J. Biomed. Mater. Res. A 105 (10) (2017) 2670–2684.

[16] D.E. Muylaert, G.C. van Almen, H. Talacua, J.O. Fledderus, J. Kluin, S.I. Hendrikse, J.L. van Dongen, E. Sijbesma, A.W. Bosman, T. Mes, S.H. Thakkar, Early in-situ cellularization of a supramolecular vascular graft is modified by synthetic stromal cell-derived factor-1α derived peptides, Biomaterials 76 (2016) 187–195.

[17] H.F. Guo, W.-W. Dai, D.-H. Qian, Z.-X. Qin, Y. Lei, X.-Y. Hou, C. Wen, A simply prepared small-diameter artificial blood vessel that promotes in situ endothelialization, Acta Biomater. 54 (2017) 107–116.

[18] E.M. Anderson, B.J. Kwee, S.A. Lewin, T. Raimondo, M. Mehta, D.J. Mooney, Local delivery of VEGF and SDF enhances endothelial progenitor cell recruitment and resultant recovery from ischemia, Tissue Eng. Part A 21 (2015) 1217–1227.

[19] M.S. Lee, T. Ahmad, J. Lee, H.K. Awada, U. Wang, K. Kim, H. Shin, H.S. Yang, Dual delivery of growth factors with coacervate-coated poly(lactic-co-glycolic acid) nanofiber improves neovascularization in a mouse skin flap model, Biomaterials 124 (2017) 65–77.

[20] C.-H. Yao, K.-Y. Chen, M.-H. Cheng, Y.-S. Chen, C.-H. Huang, Effect of genipin crosslinked chitosan scaffolds containing SDF-1 on wound healing in a rat model, Mater. Sci. Eng. C 109 (2020), 110368.

[21] X. Chen, J. Wang, Q. An, D. Li, P. Liu, W. Zhu, X. Mo, Electrospun poly(l-lactic acid-co-ε-caprolactone) fibers loaded with heparin and vascular endothelial growth

factor to improve blood compatibility and endothelial progenitor cell proliferation, Colloids Surf. B Biointerfaces 128 (2015) 106–114.

[22] Y. Chen, Z. Yuan, W. Sun, M. Shafiq, J. Zhu, J. Chen, H. Tang, L. Hu, W. Lin, Y. Zeng, L. Wang, L. Zhang, Y. She, H. Zheng, G. Zhao, D. Xie, X. Mo, C. Chen, Vascular endothelial growth factor-recruiting nanofiber bandages promote multifunctional skin regeneration via improved angiogenesis and immunomodulation, Adv Fiber Mater. ⟨https://doi.org/10.1007/s42765-022-0022 6-8⟩.

[23] M. Yu, J. Huang, T. Zhu, J. Lu, J. Liu, X. Li, X. Yan, F. Liu, Liraglutide-loaded PLGA/gelatin electrospun nanofibrous mats promote angiogenesis to accelerate diabetic wound healing via the modulation of miR-29b-3p, Biomater. Sci. 8 (2020) 4225.

[24] A. Adini, I. Adini, E. Grad, Y. Tal, H.D. Danenberg, P.M. Kang, B.D. Matthews, R. J. D'Amato, The prominin-1-derived peptide improves cardiac function following ischemia, Int. J. Mol. Sci. 22 (10) (2021) 5169.

[25] S.A. Eming, P. Martin, M. Tomic-Canic, Wound repair and regeneration: mechanisms, signaling, and translation, Sci. Transl. Med. 6 (265) (2014) 265sr6.

[26] S.H. Park, H.J. Ju, Y.B. Ji, M. Shah, B.H. Min, H.S. Choi, S. Choi, M.S. Kim, Endogenous stem cell-based in situ tissue regeneration using electrostatically interactive hydrogel with a newly discovered substance P analog and VEGF-mimicking peptide, Small, 17(40), 2103244.

[27] S.-S. Noh, S.H. Bhang, W.-G. La, S. Lee, J.-Y. Shin, Y.-J. Ma, H.-K. Jang, S. Kang, M. Jin, J. Park, B.-S. Kim, A dual delivery of substance P and bone morphogenetic protein-2 for mesenchymal stem cell recruitment and bone regeneration, Tissue Eng. Part A 21 (7–8) (2015) 1275–1287.

[28] P.Z. Costa, R. Soares, Neovascularization in diabetes and its complications. Unraveling the angiogenic paradox, Life Sci. 92 (22) (2013) 1037–1045.

[29] S. Alven, S. Peter, Z. Mbese, B.A. Aderibigbe, Polymer-based wound dressing materials loaded with bioactive agents: potential materials for the treatment of diabetic wounds, Polymers 14 (4) (2022) 724.

[30] S.Y. Rabbany, J. Pastore, M. Yamamoto, T. Miller, S. Rafi, R. Aras, M. Penn, Continuous delivery of stromal cell-derived factor-1 from alginate scaffolds accelerates wound healing, Cell Transpl. 19 (2010) 399–408.

[31] J.S. Choi, K.W. Leong, H.S. Yoo, In vivo wound healing of diabetic ulcers using electrospun nanofibers immobilized with human epidermal growth factor (EGF), Biomaterials 29 (2008) 587–596.

[32] A. Adini, I. Adini, E. Grad, Y. Tal, H.D. Danenberg, P.M. Kang, B.D. Matthews, R. J. D'Amato, The prominin-1-derived peptide improves cardiac function following ischemia, Int. J. Mol. Sci. 22 (10) (2021) 5169.

[33] J. Wen, J.Q. Zhang, W. Huang, Y. Wang, SDF-1α and CXCR4 as therapeutic targets in cardiovascular disease, Am. J. Cardiovasc. Dis. 2 (1) (2012) 20.

[34] M. Rafique, T. Wei, Q. Sun, A.C. Midgley, Z. Huang, T. Wang, M. Shafiq, D. Zhi, J. Si, H. Yan, D. Kong, K. Wang, The effect of hypoxia-mimicking responses on improving the regeneration of artificial vascular grafts, Biomaterials 271 (2021), 120746.

[35] Z. Feng, S. Qu, C. Zhang, P. Huang, H. Song, A. Dong, D. Kong, W. Wang, Bioinspired nanofibrous glycopeptide hydrogel dressing for accelerating wound healing: a cytokine-free, M2–type macrophage polarization approach, Adv. Funct. Mater. 30 (52) (2020) 2006454.

[36] M. Shafiq, Y. Chen, R. Hashim, C. He, Z. Mo, X. Zhou, Reactive oxygen species-based biomaterials for regenerative medicine and tissue engineering application, Front. Bioeng. Biotechnol. 9 (2021), 821288.

[37] A. Mohandas, B.S. Anisha, K.P. Chennazhi, P. Jayakumar, Chitosan–hyaluronic acid/VEGF loaded fibrin nanoparticles composite sponges for enhancing angiogenesis in wounds, Colloids Surf. B Biointerfaces 127 (2015) 105–113.